Tris(2,2,2-trifluoroethyl) phosphite as an electrolyte additive for high-voltage lithium-ion batteries using lithium-rich layered oxide cathode

Julie Pires, Aurore Castets, J. Santos-Peña, E. Dumont, S. Levasseur, C. Tessier, Rémi Dedryvère, M. Anouti, Laure Timperman

Tris(2,2,2-trifluoroethyl) phosphite as an electrolyte additive for high-voltage lithium-ion batteries using lithium-rich layered oxide cathode

Julie Pires[a], Aurore Castets[b], Laure Timperman[a], Jesùs Santos-Peña[a], Erwan Dumont[c], Stéphane Levasseur[d], Cécile Tessier[c], Rémi Dedryvère[b], Mériem Anouti[a] *

(a) Université François Rabelais, Laboratoire PCM2E (EA 6299), Parc de Grandmont 37200 Tours (France)

(b) IPREM (UMR 5254 CNRS), Université de Pau et des Pays de l'Adour, Hélioparc, 2 Avenue Pierre Angot, 64053 Pau Cedex 9 (France)

(c) SAFT, 111 Boulevard Alfred Daney, 33074 Bordeaux Cedex, France

(d) UMICORE, Broekstraat 31, 1000 Brussels, Belgium

* Corresponding author: E-mail: meriem.anouti@univ-tours.fr, Tel: +33(0)247366951, Fax: +33(0)247367073.

Abstract

In this paper, we report positif effect of Tris(2,2,2-trifluoroethyl) phosphite (TTFP) as additive during initial activation and cycling of Li-rich-NMC xLi_2MnO_3–$(1-x)LiMO_2$ ($x >> 1$; M = Ni, Co, Mn) cathode in EC/DMC + 1 M $LiPF_6$ electrolyte. Firstly conductivity and viscosity of electrolyte with *x* wt.% TTFP ; 0 wt.% < *x* < 20 wt.% were sudied. From the electrochemical characterization using cyclic voltammetry, galvanostatic charge/discharge and EIS we show that TTFP passives aluminum current collector and the acts as oxygen scavenger during the extended activation plateau up 4.7 V *v.s* Li^+/Li (up to 301 mAh g^{-1} in charge). The beneficial effect of TTFP improves the long-term cycling stability of the cathode with more than 95% of initial capacity in Gr // Li-Rich -NMC full cell is maintained after 50 cycles at C rate. Finally, XPS analysis of Li-Rich -NMC electrodes show presence of TTFP on the surface during cycling and confirm the presence of Mn^{3+} at the end of discharge. The convergence of all characterizations indicates that TTFP should act as a catalyst to several surface reactions which are beneficial to long cycling cell performances.

Keywords: Li-Rich –NMC, phosphite, additive, Li-ion battery, high-voltage, cathode activation.

1. Introduction

Development of high-energy cathode materials is critical for advanced lithium ion batteries that can be deployed for vehicle electrification [1-10]. Compared to the traditional cathodes such as $LiMn_2O_4$ spinel and layered $LiCoO_2$, the series of new type of lithium- and manganese-rich layer structured cathode material (named LR-NMC hereafter), having high capacity, low cost, and high energy, has attracted extensive attentions [11-21]. $Li_{1+x}(Ni_yMn_zCo_{1-y-z})_{1-x}O_2$, have so far demonstrated the highest discharge capacity (typically around 250 mAh g^{-1}) along with cost reduction and safety enhancement [11, 12, 17, 18]. However, capacity degradation and voltage fading remain the major challenges for LR cathodes prior to their practical applications. The structural details of these materials represented by $Li_{1+x}(Ni_yMn_zCo_{1-y-z})_{1-x}O_2$ formula, have been under heated debate, i.e., whether they are "real uniform solid solution" without phase separation [11, 14, 19, 20] or "composite" compounds in which layered Li_2MnO_3 and $Li(Co,Ni,Mn)O_2$ domains are structurally integrated on nanoscale with a shared common oxygen sublattice (better described as $Li_2MnO_3 \cdot Li(Co,Ni,Mn)O_2$) [16, 21-26]. Anyway, after activation of LR cathode in the initial charge process up to 4.8 V of cut-off voltage, a discharge capacity greater than 250 mAh g^{-1} can be achieved for these layered composite cathodes. There have been various explanations as to why the excess Li enhances the capacity of these materials. The high reversible capacity of the first cycle (up to more than 300 mAh g^{-1}) can be attributed to the so-called mechanism of electrochemical activation. [2, 24, 27, 28]. It has been proved by Differential Electrochemical Mass Spectrometry (DEMS) that the active material releases gaseous oxygen during this step [29]. The amount of released oxygen, however, is not sufficient to explain the great capacities. It was thus proposed that the material's oxygen anions have an electrochemical activity that is responsible for the extra-capacity, *i.e.* O^{2-} anions are oxidized upon charge and reversibly reduced upon discharge [30, 31]. Although not responsible for the high reversible capacities, the loss of oxygen from the

electrode has been proved. This irreversible phenomenon results in dramatic changes of the electrode surface structure, formation of micro-cracks at the surface and distortion of crystal periodicity [21, 26-28]. Therefore, material phase transformations (bulk and surface) are considered as one primary factor contributing to the voltage instability, capacity fading, and poor rate performance of the Li- and Mn-rich layered oxides [15, 32-34]. In addition, high cut-off voltages (4.6 - 4.8 V) are required for the material's activation, that is beyond the stability of usual carbonate-based electrolytes and unavoidably initiates electrolyte decomposition during each charge, leading either to thickening of the passivation layer on the positive electrode surface, or formation of soluble degradation species, in both cases deteriorating the electrochemical performances of LR cathodes [1, 35-38]. Layered Li-rich cathodes may provide remarkably high specific capacities, however, their practical application is still limited due to major unsolved issues, such as (i) oxygen release during initial charge, (ii) phase transformation from layered to spinel-layered intergrowth structure resulting in continuous decay of the discharge plateau during long-term cycling, (iii) transition metal dissolution in the electrolyte [39] and (iv) electrolyte oxidation during charge. To circumvent these obstacles, various strategies have been developed, especially regarding the materials synthesis. Besides some studies report on the formulation of an electrolyte suitable for this type of cathode. Several approaches have been explored, firstly, to replace the carbonate-based electrolyte to have higher anodic stability, using sulfone-based solvents, ionic liquids, dinitrile solvents or fluorinated carbonates solvents [36]. The other way is to make the carbonate-based electrolytes thermodynamically stable to high-voltage cathode using additives [35, 40, 41]. It was shown that the role of additives for high-voltage Li-ion batteries is mainly to assist the formation of stable and passivating interfacial film on the positive electrode. In this way, the decomposition of electrolyte under high potential will decrease [11]. The electrolyte plays an essential role in the stability of the material at the interface, especially at high potential in the activation cycle.

In this paper, we report on additive effect in the electrolyte to stabilise the passivation layer on the cathode surface to prevent the effects of reactions activated by the oxygen released on the cathode's surface during electrochemical cycling in order to improve stability and performance. We used Tris(2,2,2-trifluoroethyl) phosphite (TTFP) component to prevent the oxygen-related surface reactions that occur during electrochemical cycling on lithium-rich cathodes. Here, we demonstrate the direct effect of this additive on passivation of aluminum current collector and its impact as stabilising electrode surface during the extended plateau and discuss the consequences of its action on the cathode cycling.

2. Experimental

2.1. Materials

All solvents, ethylene carbonate (EC), dimethyl carbonate (DMC), Propylene carbonate (PC) and ethyl methyl carbonate (EMC) were purchased from Sigma Aldrich (purity > 99 %). Tris(2,2,2-trifluoroethyl) phosphite (TTFP) used in this study was purchased from Sigma Aldrich within a molecular purity > 99% and was used without further purification. Lithium salt, $LiPF_6$, was also purchased from Sigma Aldrich. An electrolyte of 1 M $LiPF_6$ in a binary (EC/DMC 1:1 (w/w) was selected as a reference electrolyte and quaternary (EC/PC/EMC/DMC) mixture was studied as other base of solvent for comparison. Different contents of TTFP were added in the reference electrolyte in an argon-filled glove box (M-Braun) with oxygen and water contents lower than 1 ppm. Additionally, prior to any measurement, electrolytes were analyzed for water content using coulometric Karl-Fischer (Coulometer 831 – Metrohm) titration. The water content of electrolytes used in this study is lower than 20 ± 1 ppm.

- Viscosity, conductivity and thermal measurements

Viscosity was measured using an Anton Parr digital vibrating tube densitometer (model 60/602, Anton Parr, France) and an Anton Parr rolling-ball viscometer (model Lovis 2000 M/ME,

Anton Parr, France), respectively. In both cases, the temperature in the cell was regulated within ± 0.02 °C. The uncertainty of the density and viscosity measurements were better than 5.10^{-5} g cm^{-3}, and 1 %, respectively. A Crison (GLP 31) digital multifrequency conductimeter was used to measure the ionic conductivities. The temperature control from 25 °C to 80 °C was ensured by a JULABO F25 thermostated bath with an accuracy of ± 0.2 °C. Thermal runaway of the electrolyte and charged electrodes were checked by Differential scanning calorimetry (DSC) measurements on a Perkin-Elmer DSC 4000 under a nitrogen atmosphere, coupled with an Intracooler SP VLT 100, with a flow of 10 mL min^{-1} in a temperature range from 25 to 300 °C.

- Electrochemical measurements

Electrochemical properties of the cathode material were evaluated by using coin-cells for the galvanostatic charge-discharge (GC) and Swagelok type cells for the cyclic voltammetry (CV) and impedance measurements, which were assembled in the glove-box. Li-rich-NMC xLi_2MnO_3–$(1-x)LiMO_2$ ($x>>1$; M = Ni, Co, Mn) from Umicore Belgium is used as cathode and lithium disc or graphite as the negative electrode. A double whatman GF/C glass microfiber filter (260 µm thickness and 12 mm diameter) was used as separator and drenched with 0.5 mL of electrolyte for all tests. CVs, GC and impedance were carried out using a VMP multichannel potentiostatic-galvanostatic system (Biologic Science Instrument, France). Highly pure lithium foil was used as the counter electrode and reference electrode for the cell assembly with a mass loading more than 10 times higher than that of the working electrode.

The battery performance was evaluated by galvanostatic charge-discharge tests carried out at room temperature (RT) applying a current density as a function of the working electrode mass. Impedance measurements were performed over the frequency range of 240 kHz to 5 mHz with an amplitude of 10 mV. All cells were cycled between 2 and 4.6 V at a current rate of C/20 (1C = 160 mA g^{-1}) for the first cycle. Subsequent cycles were performed at a current rate of

C/10. Electrochemical stability of electrolytes was measured by CV between 2 and 4.8 V at a scan rate of 20 μV s^{-1}.

- XPS measurements

XPS measurements were carried out with a Kratos Axis Ultra spectrometer, using a focused monochromatized Al Kα radiation ($h\upsilon$ = 1486.6 eV). The XPS spectrometer was directly connected to an argon dry box through a transfer chamber, to avoid moisture/air exposure of the samples. The spectrometer was calibrated using the photoemission line Ag $3d_{5/2}$ (binding energy 368.3 eV). For the Ag $3d_{5/2}$ line, the full width at half-maximum (fwhm) was 0.58 eV under the recording conditions. The analysed area of the samples was 300 x 700 μm^2. The analyzing depth of the XPS experiment was about the first 5 nm of the surface of the electrode. Peaks were recorded with constant pass energy of 20 eV. The pressure in the analysis chamber was around 1 x 10^{-9} Pa. Short acquisition time spectra were recorded before and after each experiment and compared to check that the samples did not suffer from degradation under X-ray beam during measurements. The binding energy (BE) scale was calibrated from the hydrocarbon contamination using C 1s peak at 285.0 eV. Core peaks were analyzed using a non-linear Shirley-type background [42]. The peak positions and areas were optimized by a weighted least-squares fitting method, using 70% Gaussian, 30% Lorentzian lineshapes. Quantification of the chemical species at the surface was performed on the basis of Scofield's relative sensitivity factors [43].

2. Results and discussion

2.2.Physicochemical characterization of the electrolyte

First, to introduce the additive used in this study, tris(2,2,2-trifluoroethyl) phosphite, TTFP, its chemical structure is presented in the Scheme 1, below.

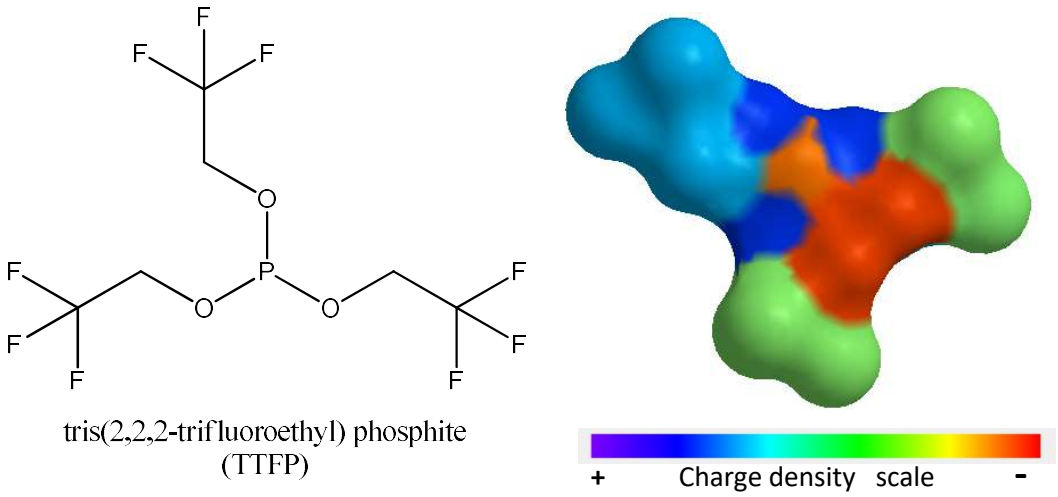

Scheme 1: Name, 3D structure and partial charge distribution of TTFP.

Oxidization number of phosphorus in TTFP is three (III) and the phosphorus center atom bears a pair of lone-pair electron [44]. This low oxidation number of phosphorus is very effective to improve the stability of $LiPF_6$-based electrolytes by complexing the hexafluorophosphate anion. TTFP was previously reported as flame-retardant in Li-ion batteries, either as additive (5 wt.%) [45] or as co-solvent (5 to 30 wt.%) [44]. Besides, it was shown that a similar structure containing the phosphate group (the species called TFP) is also a good flame-retarding when using as additive or co-solvent in Li-ion batteries [46, 47].

Physico-chemical properties, as conductivity and viscosity of electrolytes containing TTFP or TTFP-free are measured in presence of $LiPF_6$ salt, values are summarized in the Table 1 for T = 25 °C and 60 °C . $LiPF_6$ has been proved to be insoluble in TTFP as pure solvent due to a low dielectric constant [44] , whereas, (EC/DMC + x TTFP) mixtures (x = 5 wt. % and 20 wt. %) modified notably the solubility and impact consequently conductivity of EC/DMC 1 M $LiPF_6$ electrolyte. Thus, conductivity decreases by up to 10 % and 23 % by addition of 5 wt. % and 20 wt. % of TTFP respectively. This can be explained by the low dielectric constant (i.e. polarity) of TTFP, which inhibits dissociation of the salt [44]. Besides, as expected, viscosities

are also influenced by the TTFP content. From Table 1, it is visible logically, that viscosity of each electrolyte decreases with the temperature, pure TTFP presenting the lowest viscosity with 1.44 mPa s and 0.88 mPa s at 25 and 60 °C, respectively by comparison carbonate-based electrolytes which show twice higher values. Thus, the addition of 5 wt. % in EC/DMC 1M $LiPF_6$, decreases the viscosity compared to the reference electrolyte. However, when adding up to 20 wt. % of TTFP, the opposite effect is observed. This higher viscosity observed for relatively high content of TTFP can be explained by the high interaction of TTFP with carbonate as an oxygen trap phosphorous derivative, decreasing by consequence their mobility.

Table 1. Decomposition temperature (T_D), conductivity (σ), viscosity (η), density (ρ) and walden product (W) of electrolytes at 25 and 60 °C.

Electrolytes	T_D (°C)	σ (mS cm^{-1})		η (mPa s)		W ($\sigma.\eta^{-1}$)	
		25°C	*60°C*	*25°C*	*60°C*	*25°C*	*60°C*
TTFP	*nd*	0	0	1.44	0,88	*nd*	*nd*
EC/DMC 1M $LiPF_6$	145	12.29	20.90	3.26	1.78	3.77	11.74
EC/DMC 1M $LiPF_6$ + 5 wt.% TTFP	151	11.22	18.66	2.95	1.57	3.80	11.88
EC/DMC 1M $LiPF_6$ + 20 wt.% TTFP	173	9.17	15.80	3.37	1.78	2.72	8.87

Walden product, which combines conductivity and viscosity, is the most objective way to compare electrolytes. Walden product, $\sigma.\eta^{-1}$, is related to ions diffusion taking into account ionic mobility and fluidity (η^{-1}). Indeed, when W is high, electrolyte performances should be improved at high charge/discharge rate. In this way, according to values calculated in the Table 1, reference electrolyte and 5 wt.% TTFP based electrolyte are comparable, meaning that when adding 5 wt.% of TTFP, transport properties are not a lot affected, but slightly higher than the reference electrolyte. However, when adding higher content of TTFP, 20 wt.%, transport properties are strongly affected, as the Walden product is 1.3 times lower than the two other

electrolytes. Therefore it is obvious that addition of TTFP in electrolyte could have beneficial effect, according to thermal and transport properties studied here, however, the content should be controlled, and probably not exceed 5 wt.%.

2.2. Electrochemical characterization of electrolyte

- ***Corrosion test of aluminum collector in TTFP-based electrolyte***

In this study, it's important to observe the corrosion of the aluminum current collector, because performance of the system is directly linked to the stability of the current collector. In general aluminum is used as current collector for positive electrodes in Li-ion systems because of its lightness (ρ = 2.7 g cm^{-3}), its good electric conductivity, $37.7.10^6$ S cm^{-1}, and its high resistance to corrosion [48]. However aluminum is unstable at high potential with redox potential of Al/Al^{3+} couple at 2.33 V *vs*. Li^+/Li. But, it is well known that aluminum forms spontaneously passivation layer in contact with air. This thin layer, formed with Al_2O_3, is an efficient protection against corrosion. Fig. 1a shows CVs recorded on aluminum for the three selected electrolytes, the reference one, EC/DMC 1M $LiPF_6$, and with addition of 5wt. % and 20 wt. % of TTFP. We note in zoom Fig 1b, that for reference (EC/DMC 1M $LiPF_6$) low corrosion current which does not exceed 0.4 µA cm^{-2} is detectable ($i_{(peak)}$ = 0,31 µA.cm^2) (black). While, in presence of 5 wt. % TTFP, no corrosion is observed and the current densities of base line (red) is linear. It can be concluded that in both considered media, stable passivation layer is formed on aluminum with better efficiency in presence of 5 wt. % TTFP.

Considering 20 wt. % TTFP based electrolyte, corrosion current densities are increased from 3.5 V *vs* Li^+/Li, and this corrosion increases during return scan as showed by blue curve from Fig. 1a. This can be explained by the dissolution of $Al[X]_n$ species, X is anion in solution, which forms the passivation layer. At high proportions, TTFP can react with protective AlF_3 film formed at the first cycle, improving the solubility of these species in the electrolyte and dissolving therefore the passivation layer. This feature has been previously reported with PC

(propylene carbonate) as solvent [49]. In other word, it can be concluded that TTFP can be used as an additive EC/DMC 1M $LiPF_6$ without negative effect on aluminum passivation, provided TTFP content does not exceed 5 wt.% in the electrolyte mixture.

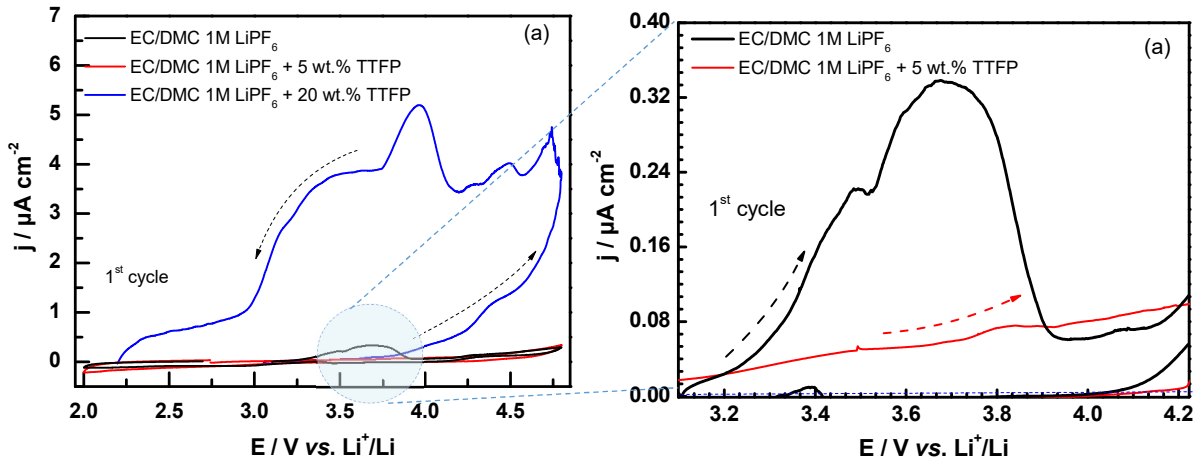

Figure 1. Cyclic voltammograms on aluminum with EC/DMC 1M $LiPF_6$ (black), EC/DMC 1M $LiPF_6$ + 5 wt.% TTFP (rouge), EC/DMC 1M $LiPF_6$ + 20 wt.% TTFP (blue), at 20 µV s^{-1}, at room temperature.

To confirm these conclusions, X-ray photoelectron spectroscopy (XPS) characterisation of the positive electrode surface was carried out after cycling with 5 wt. % TTFP to check the presence of aluminum. Indeed, in case of aluminum corrosion, dissolved Al may be detected by XPS at the surface of the positive electrode after cycling. In our case no Al could be detected after 165 cycles. After 280 cycles, a very weak Al 2p peak could be detected that corresponds to a very weak Al amount of 0.1 % (see Figure S1, supporting information).

- ***Cyclic voltammetry measurements of Li-rich electrode in half cell system***

Fig. 2 shows the CVs recorded in the half cell Li//LR-NMC with the three electrolytes at the first (a) and second (b) cycles comparing the reference electrolyte with the one containing 5 and 20 wt.% of TTFP, at room temperature. For the first cycle, two anodic peaks can be highlighted, for the three electrolytes, at 4.2 V and 4.6 V *vs.* Li^+/Li, respectively. These

preliminary results confirmed the presence of three electrochemical processes, previously described [5, 32].

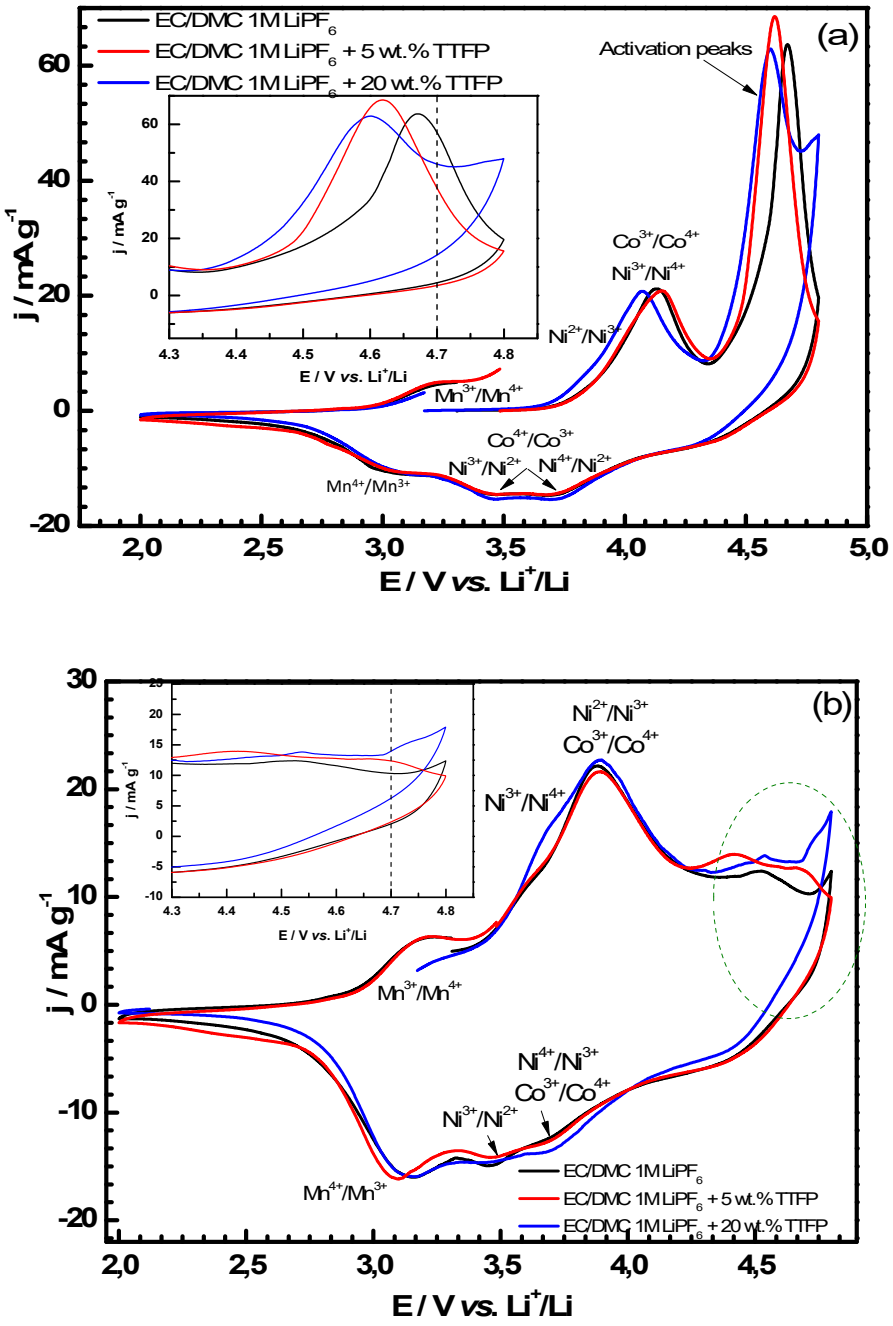

Figure 2. CVs of (a) first cycle, (b) second cycle for Li//LR-NMC half-cells with EC/DMC 1M $LiPF_6$ (black), EC/DMC 1M $LiPF_6$ + 5 wt.% TTFP (red), EC/DMC 1M $LiPF_6$ + 20 wt.% TTFP (blue), between 2 V and 4,8 V *vs*. Li^+/Li at 20 µV s^{-1}, at room temperature.

The first peak at 4.2 V *vs*. Li^+/Li is associated to Co^{4+}/Co^{3+}, Ni^{3+}/Ni^{2+} and Ni^{4+}/Ni^{3+} couples and the third peak at 4.6 V *vs*. Li^+/Li is associated to the irreversible electrochemical activation of the electrode material. The cut-off voltage of 4.8 V *vs*. Li^+/Li seems to be a good working potential regarding the good level of material activation, for the three electrolytes studied here. However, at potential above 4.7 V *vs*. Li^+/Li the CV recorded on the electrolyte containing 20 wt.% of TTFP, shows a small additional redox process after the end of the activation. This is more evident in the inset of the Fig. 2a. Upon discharge, four cathodic peaks are observed. The first one at 4.4 V can be assigned to the reversible process at the origin of the extra capacity of these materials and is not directly involving classical reduction of transition metals of the material (still under debate in the literature). The two peaks at 3.7 and 3.5 V are assigned to reduction of nickel and cobalt. Finally, an additional cathodic peak at 3.0 V, partially due to the manganese reduction at the extreme surface of the material, is observed during the first discharge process as will be demonstrated below by XPS.

In the second cycle (Fig. 2b), three peaks related to the oxidation of manganese, nickel and cobalt are now visible during the oxidation, at (3.2, 3.7 and, 3.9 V) and oxidation of species activated during the first cycle at 4.5 V *vs*. Li^+/Li respectively. As the activation process only occurs in the first cycle, no peak associated to further electrochemical activation are visible in this second cycle. The reduction shows four peaks at respectively 3, 3.5, 3.75, and 4.4 V *vs*. Li^+/Li attributed to the mono electronic reduction of transition metals. Comparing the first and the second cycles, for the discharge, the capacity due to the Mn^{4+}/Mn^{3+} couple (estimated by integration of the CV peak) is higher for the second than the first cycle. Besides, the additional peak at 4.7 V *vs*. Li^+/Li, in presence of 20 wt.% of TTFP, is always visible as observed during the charge. To reduce competitive redox processes occurring at this potential, a cut off potential as 4.7 V *vs*. Li^+/Li can be an alternative limit potential for the activation mainly for the 20 wt.% of TTFP electrolyte, as the activation is effective at this potential, for this reason, we selected

this limit of potential for further investigations. In subsequent cycles no significant difference was observed between the evolution of CVs with and without TTFP (Figure S2 in the supporting information).

In order to further investigate the redox processes involving transition metals upon charge and discharge, positive electrodes extracted from half cells cycled with EC/PC/EMC/DMC + 1M $LiPF_6$ + 5 wt. % TTFP electrolyte were analyzed by XPS. Batteries were stopped at different selected voltage points of the first cycle, opened in glove box, and positive electrodes were extracted and washed with DMC in order to remove the salt before analysis. Fig. 3 presents Li 1s and *M* 3p (*M* = Ni, Co, Mn) XPS spectra of positive electrodes at different steps of the first cycle: before cycling (Fig. 3.1), in charge (4.6 V and 4.7 V, Fig. 3.2 and 3.3, respectively) and in discharge (3.15 V and 2 V, Fig. 3.4 and 3.5, respectively).

For the starting electrode (Fig. 3a.1), Ni, Co and Mn ions are in their +II, +III and +IV valence states, respectively. Li 1s peak on Fig. 3a consists of two components: the most intense at 54.5 eV (colored in red in the figure) corresponds to Li^+ ions in the active material structure whereas the weaker peak around 55.6 eV is attributed to surface lithiated species. Upon the first charge some changes are observed.

For a better interpretation of spectra, the expected positions of Ni^{4+} and Ni^{2+} (as proposed in literature) [50] are indicated. Peak attributed to Ni^{2+} ion (~ 67.5 eV) before cycling moves towards higher binding energy (~ 68.9 eV) upon charge following its oxidation into Ni^{4+}. At this stage, Mn^{4+} ions do not show any change in the Mn 3p peak during first charge (neither in the Mn 2p spectra, not shown here). Upon discharge, the Ni 3p signal shifts back to its initial binding energy (~ 67.5 eV) at 3.15 V (Fig. 3a.4). Ni^{4+} ions are thus reduced before 3.15 V as suggested above by CV (Fig. 2).

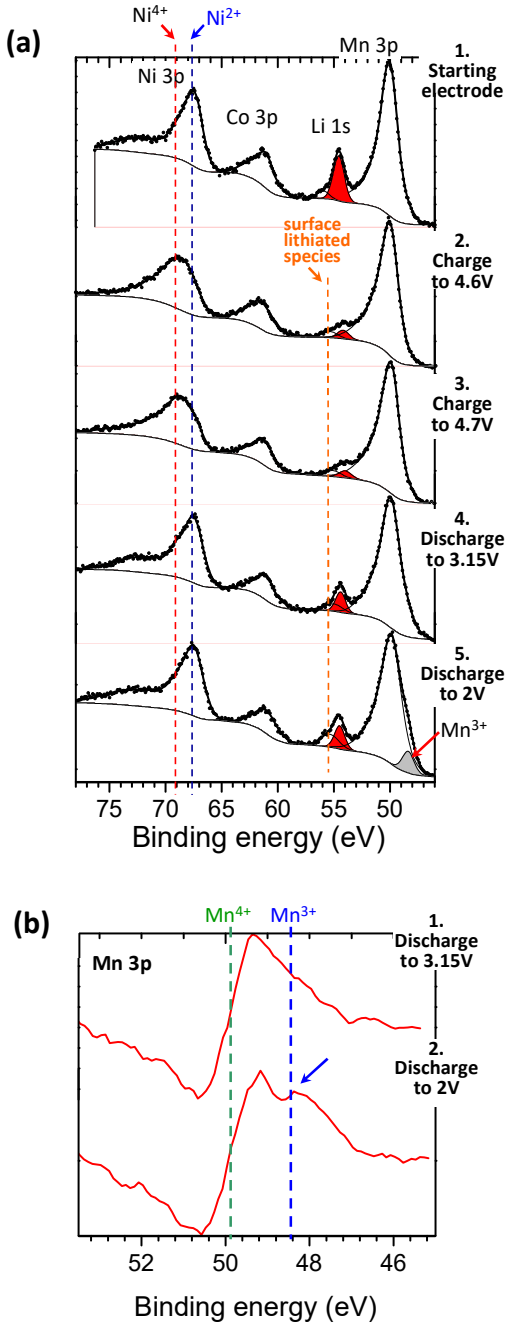

Fig. 3. (a) Ni 3p, Co 3p, Li 1s and Mn 3p XPS spectra of positive electrodes cycled in half cells with EC/PC/EMC/DMC + 1 M $LiPF_6$ + 5 wt. % TTFP electrolyte: (1) starting electrode (before cycling), electrodes charged up to (2) 4.6 V and (3) 4.7 V and electrodes charged up to 4.7 V then discharged down to (4) 3.15 V and (5) 2 V. **(b)** Derivative of Mn 3p spectra of the discharged samples at (1) 3.15 V and (2) 2 V.

Concerning Mn ions, Mn 3p peak undergoes some change during discharge. Indeed, even if no change is observed at 3.15 V (Fig. 3a.4), an additional peak can be distinguished at 2 V

(Fig. 3a.5) as a shoulder in Mn 3p peak. This peak appears at lower energy, and is attributed to Mn^{3+}. In order to better evidence this Mn^{3+} peak, a derivative of this part of the spectrum has been plotted for the two samples obtained upon discharge and is presented on Fig. 3b. For better clarity, peak positions of Mn^{4+} and Mn^{3+} have been indicated by dashed lines in figure 3b. No Mn^{3+} can be detected at 3.15 V whereas the presence of an additional derivative peak confirms the presence of Mn^{3+} at the end of discharge (2 V). This observation corroborates the results of CV (Fig. 2) showing appearance of a redox activity of Mn^{3+}/Mn^{4+} couple upon the first discharge (after 3.15 V and before the end of discharge at 2 V).

- ***Galvanostatic charge-discharge performances***

The comparative performance of lithium half-cells containing (EC/DMC + 1 M $LiPF_6$) as reference electrolyte with different amount of TTFP (0, 5, 20) wt. %, and (EC/PC/EMC/DMC + 1 M $LiPF_6$) as modified electrolyte with minimum weight content of TTFP as 0.5 wt. % for comparison are shown in Fig. 4. The (a, b) series compares TTFP effect on the cyclability at two first charge discharge cycles in half cell system, while (c, d) series considers the cycling ability of full cell at C rate during the first hundred cycles. In all cases, activation is performed at a rate of C/10, and following cycles at a rate of C/5. During the charge, two plateaus are visible between the start and 4.3 V and between 4.3 V and 4.6 V.

In Fig. 4a we can recognize the features already discussed by CV from Fig. 2. The primary plateau 4.1 V can be associated to the oxidation of Ni^{2+} into Ni^{3+} and Ni^{4+} and Co^{3+} into Co^{4+}. The large plateau at 4.5 V can be associated to the activation process of the electrode material. In the discharge these features are less visible. No difference was observed in charge discharge profile obtained in the binary or quaternary based solvent of electrolyte.

The slope from 4.6 V to 3.3 V corresponds to the reversible part of the extra capacity (redox activity of oxygen) and to the reduction of cobalt and nickel.. Charge/discharge capacity values calculated from CV and GC are reported in the Table 2.

Table 2. Charge/discharge capacity calculated from cyclic voltammetry and galvanostatic charge-discharge for half-cells with EC/DMC 1 M $LiPF_6$ with TTFP (0, 5 or 20. wt %).

Method	Electrolytes EC/DMC + 1 M $LiPF_6$	Charge capacity (mAh g^{-1})		Discharge capacity (mAh g^{-1})	
		1st cycle	2nd cycle	1st cycle	2nd cycle
Cyclic voltammetry (20 µV/s)	0 wt.% TTFP	249	173	177	173
	5 wt.% TTFP	267	195	180	173
	20 wt.% TTFP	251	152	184	191
Galvanostatic C/20 ; C/10	0 wt.% TTFP	263	229	230	215
	5 wt.% TTFP	301	242	245	237
	20 wt.% TTFP	285	223	220	207

* 1st cycle C/20; 2nd cycle C/10

From these charge/discharge profiles and the observed capacities it is obvious that the 5 wt.% TTFP based electrolyte offers better capacity both in charge and discharge with 301 and 245 mAh g^{-1} in the first cycle. With 5 wt.% TTFP, the activation of the material seems to be better, at 4.6 V, giving higher capacity during the first discharge, which is 8 % more than with the reference electrolyte and 12 % more than with the 20 wt.% TTFP based electrolyte.

Besides, during activation, electrolyte containing 20 wt.% of TTFP exhibits longer activation plateau than EC/DMC based electrolyte without additive, however this behavior is not reflected by better capacity during the first discharge. It can be therefore assumed that, in this case the TTFP concentration is too high and acts negatively on the activation of LR-NMC.

During the second cycle the 5 wt.% TTFP based electrolyte maintains higher capacity than the two other electrolytes, with good capacity retention, as the capacity loss between the first and the second cycle is only 3 % when increasing the cycling rate from C/20 to C/10.

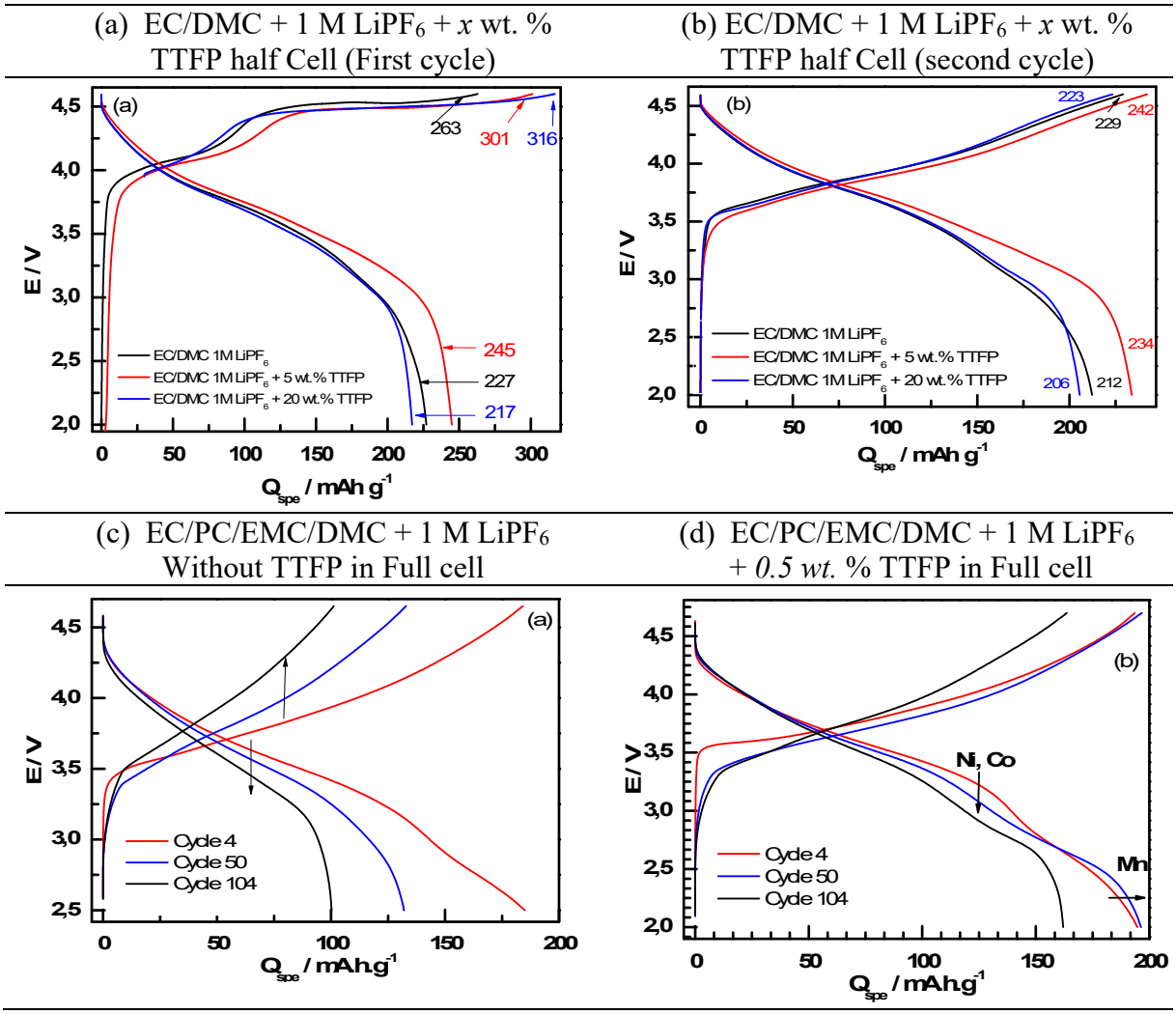

Fig. 4. Charge discharge profile of half-cells Li//LR-NMC with EC/DMC 1M $LiPF_6$ containing different among of TTFP: (a) first cycle; (b) second cycle, and full-cells Graphite//LR-NMC with EC/PC/EMC/DMC 1 M $LiPF_6$ without (c) and with (d) TTFP.

The two other electrolytes exhibit nearly the same capacity at the second cycle, around 225 mAh g^{-1} in charge and 210 mAh g^{-1} in discharge. Indeed, the effect of TTFP is more visible when it is added at 5 wt.% but, at high content, opposite effect is observed, decreasing the capacity.

In the case of full cell Graphite//LR-NMC series, because the anode of graphite is especially sensitive to the presence of additive due to the formation of the protective SEI, we have chosen in the case of whole cells to reduce the proportion of TTFP at 0.5%. In this case, the capacity retention and potential fading, which are the two markers of improved performance are showed in Fig. 4c and Fig. 4d at C scan rate. We can show from these figures that even in presence of 0.5 wt. % of TTFP, more than 95 % of initial capacity is maintained after 50 cycles, while in absence of TTFP there was a decrease in the discharge capacity close to 40 %. Charge/discharge capacity values calculated from galvanostatic charge-discharge for Graphite//LR-NMC Full cell system at C rate are reported in the Table 3.

Table 3. Charge/discharge capacity calculated from galvanostatic charge-discharge for Graphite//LR-NMC Full cell system with EC/PC/DMC/EMC 1 M $LiPF_6$ and with 0.5 wt. % TTFP.

Electrolytes	Discharge capacity (mAh g^{-1}) at C rate		
	4^{th} cycle	50^{th} cycle	104^{th} cycle
EC/PC/DMC/EMC 1 M $LiPF_6$	160	128	100
EC/PC/DMC/EMC 1 M $LiPF_6$ + 0.5 wt.% TTFP	192	190	160

* 1^{st} cycle C/20 ; 2^{nd} cycle C/10

This additive content effect was previously observed for another phosphite additive (TMP, Trimethyl phosphite) used with lithium-rich cathode [35]. Li et al. [35] showed that TMP-based electrolyte exhibits high capacity retention and good rate capability. This was attributed to the fact that TMP acts as a film-formation additive to build the passivating interphase on the surface

of the lithium-rich cathode. Therefore the presence of phosphites derivative seems to stabilize the interface between the cathode material and the electrolyte. In addition to that, Hong et al. [51] proposed the involvement of oxygen radicals in side reactions close to the surface of the electrode, and concluded that the removal of oxygen radicals is a key point for the use of lithium-rich transition metal oxides in lithium batteries.

TTFP has been reported as additive in Li/air battery [52] and performance improvement was attributed to the increased dissolution kinetics and solubility of oxygen in this phosphorus and fluorinated solvent. Therefore, higher capacity retention observed here, with 0.5 wt.% TTFP based electrolyte, could be attributed to the reaction of oxygen with TTFP in the electrolyte, which decreases the oxygen radicals involvement in side reactions and will stabilize the electrode material surface during cycling.

A phosphite containing a phosphorus atom in its non-maximal oxidation state +III easily reacts with reactive oxygenated species as (O_2; $O_2^{\cdot-}$; O_2^{2-}) to form a stable phosphate compounds that is soluble in the electrolyte (Scheme 2).

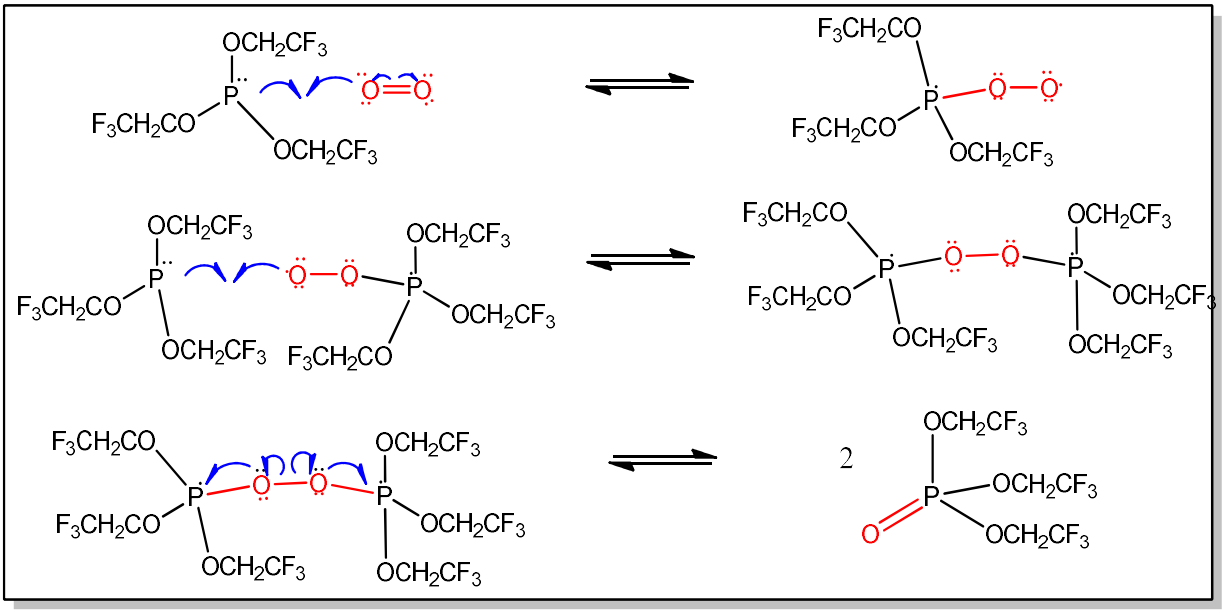

Scheme 2: Proposed mechanism to explain the TTFP reactivity with oxygen evolved out of the cathode material at activation step.

Thus, protection of electrolyte toward active oxygen could explain the best activation observed with 5 wt.% TTFP, and also the capacity retention which will be discussed below.

As an oxygen trap, the phosphorous derivative triethylphosphite (TTFP) as an additive not only leads to an improvement in the cycling performance of a full cell with the Li-rich cathode but also can lead to a decrease in the internal pressure of the cells due to decrease of side reactions of the solvents producing gases. Lee *et al* confirmed by a ^{31}P NMR and study that the use of TEP as an additive reduces the internal pressure by reacting with the oxygenated species that evolves out of the cathode material [53]. In their work, the action of phosphite additives on oxygenated species at Lithium-rich cathode, has been provided by ^{31}P nuclear magnetic resonance (NMR) spectroscopy and gas chromatography-mass spectrometry (GCeMS), which clearly show the presence of reaction products in accordance with the mechanism described here. Thus, unwanted decomposition of electrolyte solvents by O_2^- attack can be alleviated. Besides, they show that byproducts from TTFP can react with undesirable oxygenated impurities, like water. It is now admitted that this residual water negatively affects the cycle life of cell by hydrolysing the salt, forming hydrofluoric acid that attacked the surface of the electrode. Thus, the double positive effect of TTFP is both its capacity to react with oxygenated byproducts and in same time with oxygenated species formed at activation stage. As a result, the severe capacity fading of Li-rich cathodes due to these phenomenon could be prevented.

- ***Long cycle performances in presence of TTFP***

The reversible capacity *vs*. cycle number curves, showing the stability during cycling for the three studied electrolytes, with and without TTFP, is shown in Fig. 5a. The electrolyte with 5 wt.% TTFP provides the best capacity but it decreases continuously during cycling, with a capacity loss of 10 % between the second and the 30th cycle (233 to 210 mAh g^{-1}). However, the capacity loss is mainly observable during the first fifteen cycles. In fact from the 15th to the 30th cycle the capacity remains stable around 210 mAh g^{-1}. The EC/DMC 1 M $LiPF_6$ reference

electrolyte has the poorer capacity and- it decreases drastically during cycling to reach only 72 % of the initial capacity after 12 cycles, with 154 mAh g^{-1}. For the electrolyte based on 20 wt.% of TTFP, it is able to provide a rather stable capacity during the first 12 cycles. Besides, for the three electrolytes, efficiency, plotted in the Fig. 5b, is kept constant, higher than 95 %, after the 3rd cycle. However, efficiency is still higher for 5 wt.% TTFP than for 20 wt.% TTFP, this was previously observed by Li et al. [35] with TMP additive, they concluded that a possible reason of this excess charge capacity can be the oxidation decomposition of too much additive on the cathode surface. Indeed too much additive TTFP is probably not stable on the high voltage cathode.

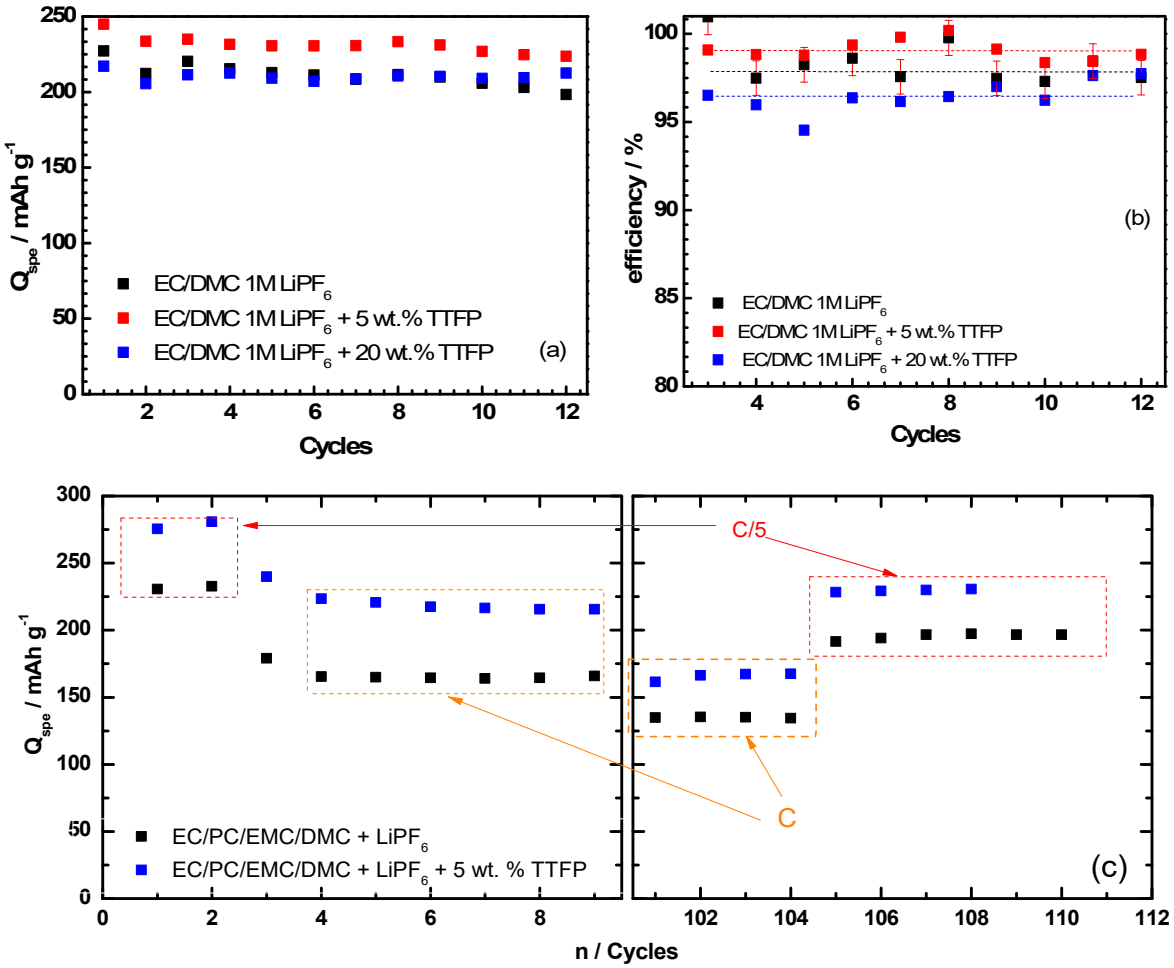

Fig. 5. Cycling performance of lithium half-cells with EC/DMC 1 M $LiPF_6$ (black), EC/DMC 1 M $LiPF_6$ + 5 wt.% TTFP (rouge), EC/DMC 1M $LiPF_6$ + 20 wt.% TTFP (blue), between 2 V and 4.6 V: (a), (c) specific capacity, (b) efficiency. First cycle at C/20 and the others at C/10.

From Fig. 5c, TTFP improves the performances with high discharge capacity up 280 mAh g^{-1} at the second cycle and maintains these performances by long-term cycling stability of Li-rich cathode up to 230 mAh g^{-1} at after 110 cycles at C/5 rate more than 30 % by comparaison with standard electrolyte. According to these results, TTFP based electrolyte is able to provide higher capacity and good capacity retention over 110 cycles than the reference EC/DMC 1 M $LiPF_6$. This could be explained by reactivity of oxygen towards TTFP in the electrolyte [52], which limits oxygen radicals reactions, as explained above, and maintains the cycling performance of the system.

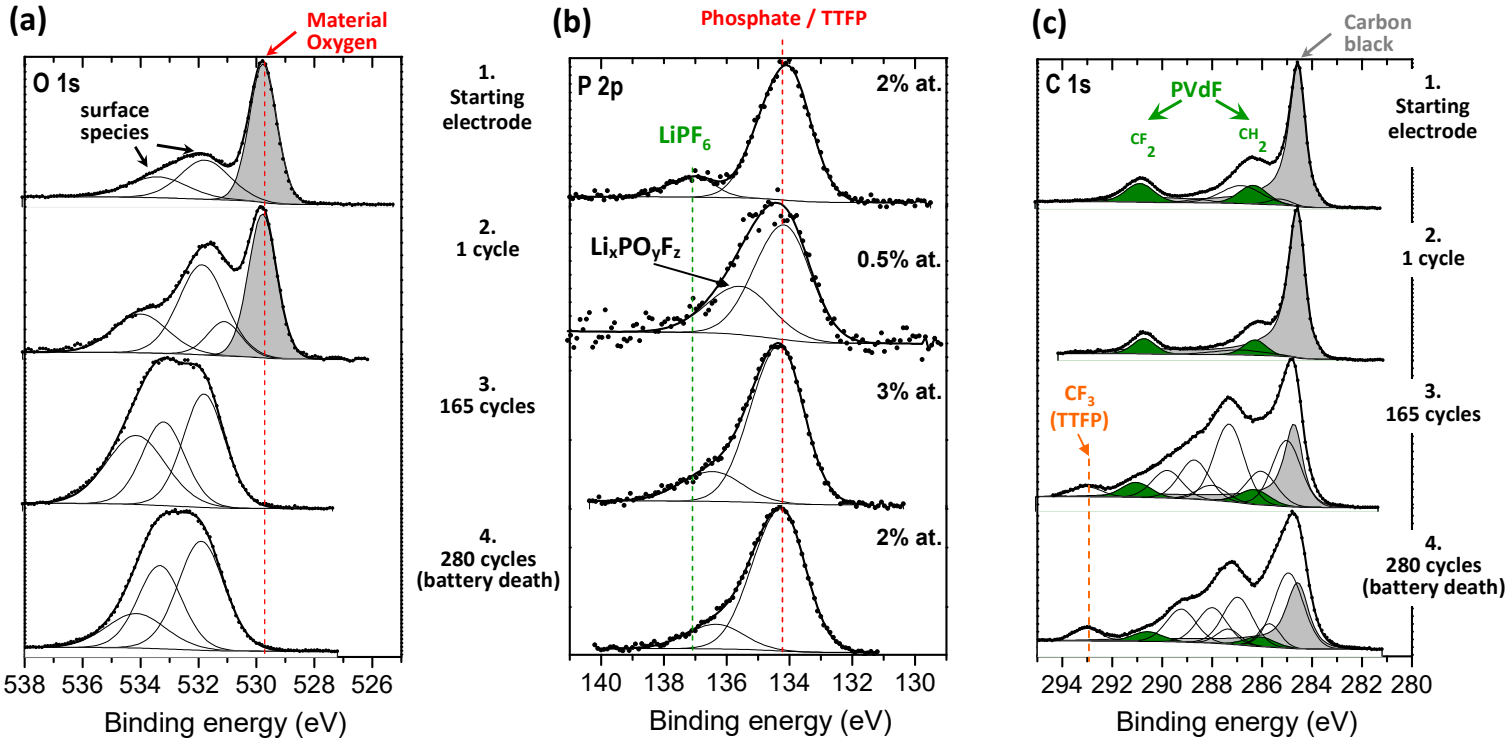

Fig. 6 (a) O 1s, **(b)** P 2p and **(c)** C 1s XPS spectra of positive electrodes (1) before cycling, and after (2) 1 cycle, (3) 165 cycles and (4) 280 cycles (corresponding to battery death), in half cells with EC/PC/EMC/DMC + 1 M $LiPF_6$ + 5 wt. % TTFP electrolyte. Amount of P 2p (% at.) is noted on P 2p spectra.

In order to better understand the action of TTFP on the active material surface, this study was complemented by XPS analysis. Fig. 6a and 6b show O 1s and P 2p spectra, respectively, of

positive electrodes before cycling and after 1, 165 and 280 cycles (battery death, C = 0 mAh.g^{-1}) with EC/PC/EMC/DMC + 1 M $LiPF_6$ + 5 wt. % TTFP electrolyte. The O 1s spectrum of the starting electrode possesses different components: the most intense peak corresponds to oxygen from active material structure (grey peak). Other weak peaks at higher binding energy correspond to adsorbed oxygenated species at the surface, and also to oxygen anions of the subsurface that have a deficient coordination[54].

After a first cycle (Fig. 6a.2) the components assigned to surface species are more intense, which can be explained by the formation of a passivation layer at the surface of the active material. After a long cycling, as can be seen on Fig. 6a.3 and 6a.4, the material oxygen cannot be observed anymore (grey peak disappeared) because of a too thick passivation layer (> 5-10 nm) covering its signal. The thickness of the passivation layer is then increasing during long cycling. However the formed film does not mainly consist of accumulation of TTFP or phosphorus-containing products. Indeed, as can be observed in Fig. 6b presenting P 2p spectra, the global amount of phosphorus at the surface of the electrode, including decomposition products of the salt $LiPF_6$, remains very low (2-3%) compared to the great amount of oxygen deposited at the surface".

The presence of TTFP on the surface during cycling can be checked on C 1s spectra of the same samples (Fig. 6b). Indeed, the signature of the TTFP CF_3 groups is clearly recognizable in the spectrum around 293 eV. The C 1s spectrum of starting electrode is presented on Fig. 6b.1. The most intense peak corresponds to the conductive carbon black at 284.9 eV (in grey on Fig. 6b.1) used in electrode composition. Two other components (in green on Fig. 6b.1) correspond to CF_2 (290.8 eV) and CH_2 (286.4 eV) groups from polymer binder PVdF in the electrode. Other weak components correspond to surface carbonaceous species. No significant difference is observed after one cycle. However, C 1s spectra of electrodes after longer cycling show great differences. They still possess the carbon black (grey peak) and PVdF (green peaks) signatures.

However, over these peaks are added intense components of carbonaceous species present in the passivation layer.

After 165 cycles and 280 cycles (Fig. 6b.3 and 6b.4), an additional peak can be observed at higher binding energy (293 eV), that can definitely be attributed to CF_3 groups from TTFP. The global amount of carbon from these CF_3 groups remains lower than 1% at the surface, which is much lower than the great amounts of oxygen deposited in, the surface film, showing again that the passivation layer does not consist of TTFP or its degradation products. Instead, TTFP should act as a catalyst to other surface reactions which are beneficial to battery performances. Long cycling is needed for TTFP or its degradation products to be trapped on electrode surface in weak amounts.

- ***Electrochemical impedance spectroscopy characterization***

In order to further investigate the formation of passivation layers at the surface of the LR-NMC material, Electrochemical Impedance Spectroscopy (EIS) were carried out upon the first charge/discharge cycle. The unsuitability of the 20 wt.% TTFP based electrolyte was confirmed by EIS measurements. Fig. 7a shows the Nyquist plots corresponding to the positive electrode charged at 4.6 V in the three different electrolyte configurations. For the reference electrolyte, a Randles classic model of equivalent circuit modified with a R//C element associated to a surface film (Fig. 7, Scheme I) allows a suitable fitting of the plots. Furthermore, the presence of TTFP enhances the corrosion of the aluminum at this voltage, producing a loop in the high frequencies region of the Nyquist plots (Fig. 7a and insets). This feature is consistent with the comparatively higher intensity developed onto the Al surface when 20 wt.% TTFP-containing electrolyte was used. The loop can be fitted by inserting several elements associated to the corrosion of the collector, mainly a corrosion film consisting of adsorbed species onto the aluminum (Fig. 7, Scheme II). Physical properties of this film (resistance, R_{film}, and

capacitance, C_{film}) are measured and collected in the Table 4, along with other electrical parameters and the fitting parameter (χ^2) issued from the fitting of the Fig. 7 curves.

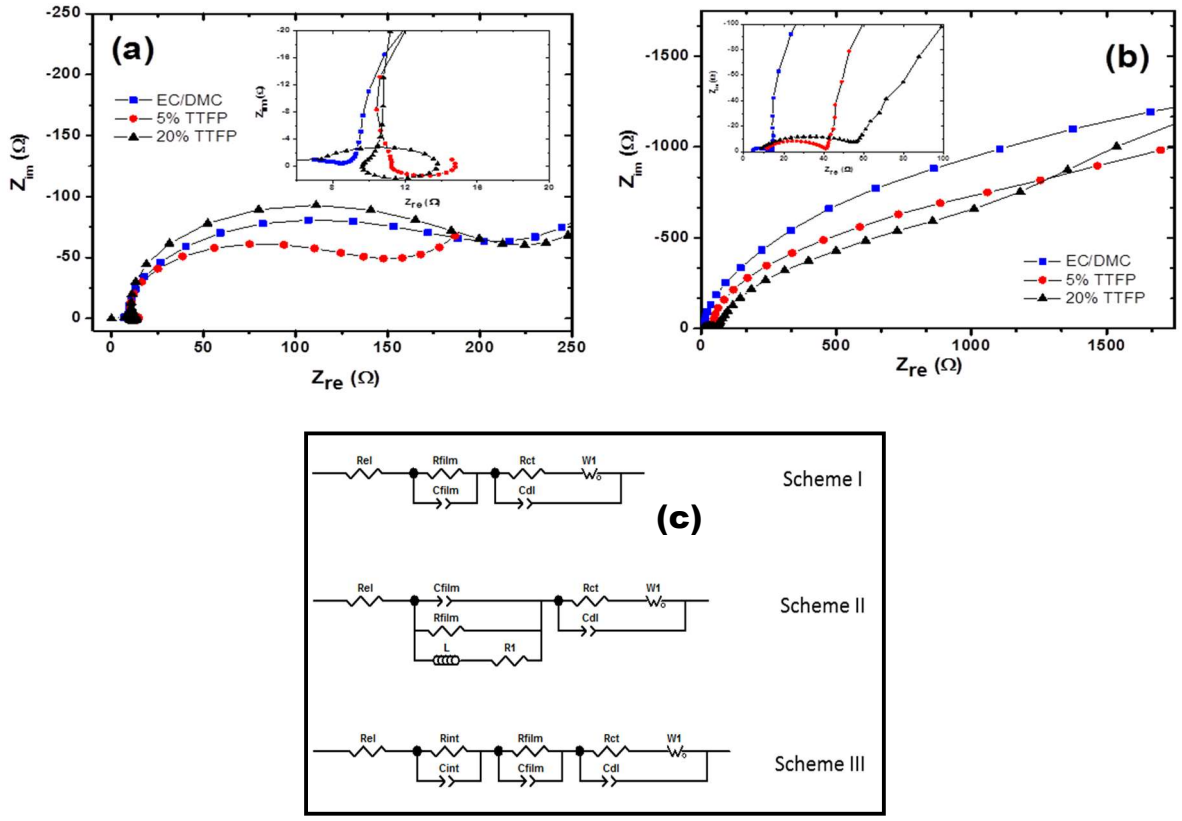

Fig. 7. Nyquist plots to the electrodes charged at 4.6 V (a) and cycled in the 4.6 - 2.0 V (b) and corresponding equivalent circuits (c), with different electrolyte configurations.

As expected from their smaller conductivities, the electrolyte resistance, R_{el}, is higher for the TTFP-containing electrolytes than for the reference electrolyte. More interesting are the surface films found for the three electrolytes. Independently on its nature (electrolyte degradation products or corrosion), the capacitances associated follow the rank: 20 wt.% TTFP > 0 wt.% TTFP >> 5 wt.% TTFP electrolytes. This finding matches the corrosion intensities and is associated to a major surface exposed to the electrolyte due to the corrosion progress. Moreover, the same rank is observed for R_{film}, indicating that a minor extension of film leads to a lesser difficulty of the electrons to transfer from the electrolyte to the positive electrode.

In spite of these interesting findings concerning the 5 wt.% TTFP electrolyte, there is some ambiguity about its role in the activation process of the cathode coming from the value of R_{ct}. From this preliminary analysis, there should not be a real activation by TTFP addition to the reference electrolyte. However the role played by the film present onto the electrode must be reminded. Its electronic resistivity hinders the access of electrons to the electrode surface where charge transfer takes place. In other words, charge transfer resistance can be increased by the presence of such resistive films. Therefore, the 5 wt.% TTFP-containing electrolyte shows the smallest value of R_{film}, accounting for the smallest value of R_{ct} in the electrolyte series.

We also measured the impedances of discharged electrodes.. Below 3.0 V vs Li^+/Li, redox process is probably associated to the formation of defects increasing the impedance of the global system. Fig. 7b contains the Nyquist plots of the discharged electrodes. Scheme III of Fig. 7, used for the fitting of the curves, is a Randles classic model modified with two R//C element that are associated to two kinds of interfacial processes. The collector/grain or the inter-grain resistances account for the first half-circle at higher frequencies. At high-middle frequencies, the second half-circle is provided by a surface film. Table 5 collects the electrical parameters obtained by fitting the Nyquist plots by using this scheme. The values of R_{ct} for the 0 and 20 wt.% TTFP electrolytes are very similar, in line with the close values of capacities shown by the half cells, their differences being more probably ascribed to higher values of R_{film} for the 20 wt.% TTFP containing electrolyte.

Table 4
Electrical parameters from the Nyquist plots of the electrodes charged up to 4.6 V.

Electrolyte	R_{el} (Ω)	R_{film} (Ω)	C_{film} (mF)	R_{ct} (Ω)	C_{dl} (mF)	χ^2
EC/DMC 1 M $LiPF_6$	4.3	4.8	$1.1 \cdot 10^{-3}$	163	7.0	0.002
EC/DMC 1 M $LiPF_6$ + 5 wt.% TTFP	11.0	3.3	$1.5 \cdot 10^{-10}$	117	11.9	0.046
EC/DMC 1 M $LiPF_6$ + 20 wt.% TTFP	7.1	6.8	$2.8 \cdot 10^{-3}$	160	7.5	0.001

Table 5
Electrical parameters from the Nyquist plots of the electrodes discharged at 2.0 V.

Electrolyte	R_{el}(Ω)	R_{int} (Ω)	C_{int} (mF)	R_{film} (Ω)	C_{film} (mF)	R_{ct} (Ω)	C_{dl} (mF)	χ^2
EC/DMC 1 M $LiPF_6$	4.0	7.0	$5 \cdot 10^{-3}$	3.0	0.10	890	2.0	0.0040
EC/DMC 1 M $LiPF_6$ + 5 wt.% TTFP	10	11	$8 \cdot 10^{-3}$	21	0.07	723	2.2	0.0007
EC/DMC 1 M $LiPF_6$ + 20 wt.% TTFP	7	15	0.1	34	0.03	842	2.0	0.0001

- ***TTFP effect on thermal stability of Li-Rich NMC and electrolyte***

As an effective fire-retardant [44, 45], TTFP represents a good thermal protector of the electrode surface. Therefore these properties were also investigated in this paper. To understand the TTFP effect on the electrolyte, and distinguish its action from this one on the active electrode material, we performed by DSC comparative thermograms in the presence of different percentages of TTFP in the electrolyte.

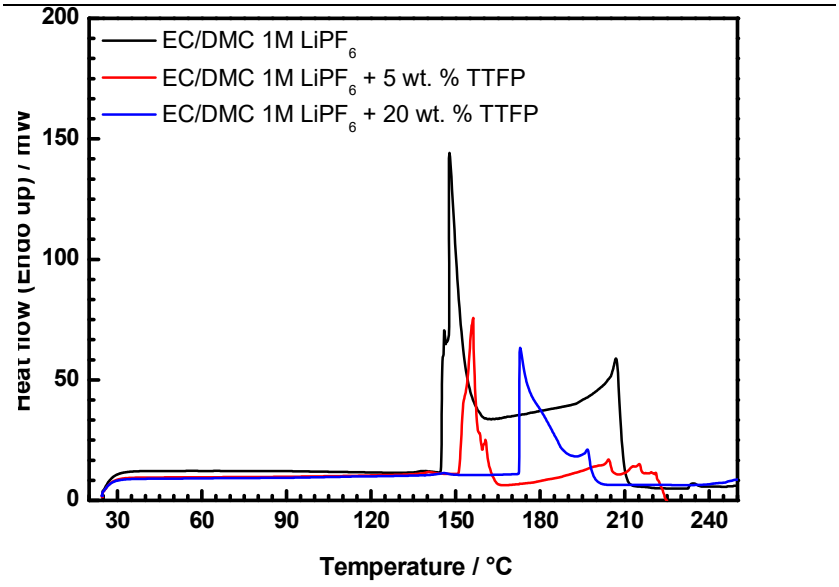

(b) Active material stability

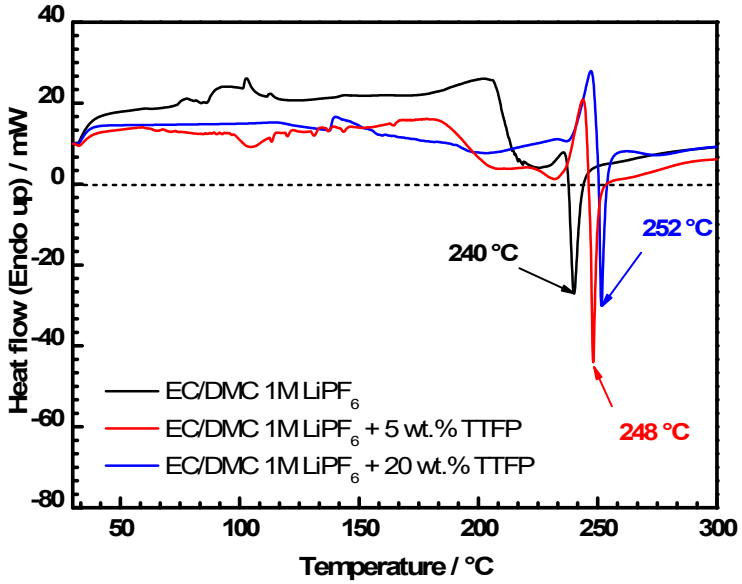

Figure 8. DSC thermograms of (a) electrolyte and (b) for the positive electrodes charged at 4.6V as function of weight percentage on TTFP in electrolyte.

Fig. 8a shows the DSC thermograms of EC/DMC 1 M $LiPF_6$, as reference electrolyte containing (0, 5, 20) wt. % of TTFP. Decomposition peaks of each electrolyte were observed at 148 °C, 155 °C and 173 °C, respectively. It is obvious that decomposition temperature increases when increasing the amount of TTFP, confirming the higher thermal stability of TTFP-containing electrolyte, compared to the reference electrolyte. In fact, decomposition peak observed here is attributed to the boiling point of DMC in the electrolyte. Therefore, the improvement of thermal stability of electrolyte containing TTFP, could be attributed to the "complexation" of DMC through the carbonate function, which will become less volatile. Comparatively, thermograms corresponding to 4.6 V charged positive electrodes under the three different electrolyte configurations as shown in Fig. 8 b, present different positions of exothermic peaks according to the amount of TTFP present in the electrolyte reflecting the interaction of electrolyte with active material.

As it has been previously reported [35, 55], the peak temperature, and heat flow have very important effect on thermal stability of lithium-ion batteries. For each thermograms a peak, characteristic of the reaction between the charged electrode surface and the electrolyte, is developed in the 225-260 °C range. Both, the onset and the maximum peak temperature are strongly depending on the amount of TTFP present in the electrolyte. Thus, the addition of TTFP increases both temperatures, confirming the protective effect of this compound when added to the electrolyte. Indeed, introduction of 5 wt. % or 20 wt.% TTFP allows the reaction to proceed, respectively, 17 °C and 28 °C up from the reference electrolyte, and shifts, respectively to 8 °C or 12 °C the maximum peak. Enthalpies values associated to the peaks in the 238-250 °C range are 92.5, 74.7 and 80.3 J g^{-1} for a content of 0, 5 and 20 wt.% of TTFP in the reference electrolyte, respectively. These values are consistent with a smaller reactivity of the charged (oxidized, highly active) positive electrode surface and this TTFP based electrolyte. The main exothermic reactions between charged electrode and electrolyte are related to the

catalytic properties of surface metal ions of the cathode [56, 57]. As it was previously reported for TMP [35], here TTFP seems to catalyse the formation of a protective film on the surface of the cathode material, and then the passivating electrolyte/cathode interphase layer could deactivate the active "catalytic" centers. Therefore, thermal stability of the charged cathode and electrolyte is enhanced by introduction of TTFP, which is clearly advantageous from a battery safety point of view.

3. Conclusions

Based on the experimental results of this study, a number of conclusions were derived. Firstly, we showed that Tris(2,2,2-trifluoroethyl) phosphite was an efficient additive in EC/DMC 1 M $LiPF_6$ as active "catalytic" centers on Li-rich-NMC. As an oxygen trap, the TTFP as additive acts as a stabilizer of oxygen on the surface as showed by XPS and EIS measurements and not only leads to an improvement in the cycling performance of a lithium half-cell or Graphite full cell with the Li-rich cathode but also can decrease the cathode material reactivity with electrolyte as showed by DSC measurement. Indeed, thermal stability of the charged cathode and electrolyte is enhanced by introduction of TTFP, which is clearly advantageous from a battery safety point of view. Furthermore, TTFP thanks to its CF_3 group, at low proportion (about 5%) and favors a redox activity of activated species since the first discharge as confirmed both by CVs and XPS spectra. By consequences TTFP improves the performances with high discharge capacity up 280 mAh g^{-1} at the second cycle and maintaisn these performances by long-term cycling stability of Li-rich cathode up to 230 mAh g^{-1} after 110 cycles.

Acknowledgments

This research was supported by "Agence National de la Recherche (ANR) " through the Alisé project.

References

[1] S. Hy, F. Felix, J. Rick, W.-N. Su, B.J. Hwang, Journal of the American Chemical Society, 136 (2014) 999-1007.
[2] M.M. Thackeray, S.-H. Kang, C.S. Johnson, J.T. Vaughey, R. Benedek, S.A. Hackney, Journal of Materials Chemistry, 17 (2007) 3112-3125.
[3] Y.-K. Sun, M.-J. Lee, C.S. Yoon, J. Hassoun, K. Amine, B. Scrosati, Adv. Mater., 24 (2012) 1192-1196.
[4] Y. Wu, A. Vadivel Murugan, A. Manthiram, J. Electrochem. Soc., 155 (2008) A635-A641.
[5] X.-J. Guo, Y.-X. Li, M. Zheng, J.-M. Zheng, J. Li, Z.-L. Gong, Y. Yang, J. Power Sources, 184 (2008) 414-419.
[6] J. Wang, X. Yao, X. Zhou, Z. Liu, J. Mater. Chem., 21 (2011) 2544-2549.
[7] A. Ito, D. Li, Y. Sato, M. Arao, M. Watanabe, M. Hatano, H. Horie, Y. Ohsawa, J. Power Sources, 195 (2010) 567-573.
[8] J. Hong, D.-H. Seo, S.-W. Kim, H. Gwon, S.-T. Oh, K. Kang, J. Mater. Chem., 20 (2010) 10179-10186.
[9] J. Zheng, J. Xiao, M. Gu, P. Zuo, C. Wang, J.-G. Zhang, J. Power Sources, 250 (2014) 313-318.
[10] K.A. Jarvis, C.-C. Wang, A. Manthiram, P.J. Ferreira, Journal of Materials Chemistry A, 2 (2014) 1353-1362.
[11] M. Hu, X. Pang, Z. Zhou, Journal of Power Sources, 237 (2013) 229-242.
[12] Y.-K. Sun, S.-T. Myung, B.-C. Park, J. Prakash, I. Belharouak, K. Amine, Nature Mater., 8 (2009) 320-324.
[13] B.J. Hwang, C.J. Wang, C.H. Chen, Y.W. Tsai, M. Venkateswarlu, J. Power Sources, 146 (2005) 658-663.
[14] K.A. Jarvis, Z. Deng, L.F. Allard, A. Manthiram, P.J. Ferreira, Chem. Mater., 23 (2011) 3614-3621.
[15] M. Gu, I. Belharouak, J. Zheng, H. Wu, J. Xiao, A. Genc, K. Amine, S. Thevuthasan, D.R. Baer, J.-G. Zhang, N.D. Browning, J. Liu, C. Wang, ACS Nano, 7 (2012) 760-767.
[16] S.C. Hamm, S. Basuray, S. Mukherjee, S. Sengupta, J.C. Mathai, G.A. Baker, S. Gangopadhyay, Journal of Materials Chemistry A, 2 (2014) 792-803.
[17] Q. Wu, S. Ha, J. Prakash, D.W. Dees, W. Lu, Electrochim. Acta, 114 (2013) 1-6.
[18] Q. Zhang, T. Peng, D. Zhan, X. Hu, J. Power Sources, 250 (2014) 40-49.
[19] Y. Wu, J. Ming, L. Zhuo, Y. Yu, F. Zhao, Electrochimica Acta, 113 (2013) 54-62.
[20] L. Li, X. Zhang, R. Chen, T. Zhao, J. Lu, F. Wu, K. Amine, Journal of Power Sources, 249 (2014) 28-34.
[21] Y. Matsuda, K. Suzuki, M. Hirayama, R. Kanno, Solid State Ionics, 262 (2014) 88-91.
[22] J. Bareño, C.H. Lei, J.G. Wen, S.H. Kang, I. Petrov, D.P. Abraham, Adv. Mater., 22 (2010) 1122-1127.
[23] J. Bareño, M. Balasubramanian, S.H. Kang, J.G. Wen, C.H. Lei, S.V. Pol, I. Petrov, D.P. Abraham, Chem. Mater., 23 (2011) 2039-2050.
[24] S. Rajarathinam, S. Mitra, R.K. Petla, Electrochim. Acta, 108 (2013) 135-144.
[25] F. Cheng, J. Chen, H. Zhou, A. Manthiram, Journal of The Electrochemical Society, 160 (2013) A1661-A1667.
[26] R.J. Gummow, N. Sharma, R. Feng, G. Han, Y. He, Journal of The Electrochemical Society, 160 (2013) A1856-A1862.
[27] S.-H. Kang, M.M. Thackeray, Electrochemistry Communications, 11 (2009) 748-751.

[28] A.R. Armstrong, M. Holzapfel, P. Novák, C.S. Johnson, S.-H. Kang, M.M. Thackeray, P.G. Bruce, Journal of the American Chemical Society, 128 (2006) 8694-8698.
[29] J.M. Zheng, Z.R. Zhang, X.B. Wu, Z.X. Dong, Z. Zhu, Y. Yang, Journal of The Electrochemical Society, 155 (2008) A775-A782.
[30] H. Koga, L. Croguennec, M. Ménétrier, K. Douhil, S. Belin, L. Bourgeois, E. Suard, F. Weill, C. Delmas, Journal of The Electrochemical Society, 160 (2013) A786-A792.
[31] M. Sathiya, G. Rousse, K. Ramesha, C.P. Laisa, H. Vezin, M.T. Sougrati, M.L. Doublet, D. Foix, D. Gonbeau, W. Walker, A.S. Prakash, M. Ben Hassine, L. Dupont, J.M. Tarascon, Nat Mater, 12 (2013) 827-835.
[32] C.S. Johnson, N. Li, C. Lefief, J.T. Vaughey, M.M. Thackeray, Chemistry of Materials, 20 (2008) 6095-6106.
[33] A. Ito, K. Shoda, Y. Sato, M. Hatano, H. Horie, Y. Ohsawa, J. Power Sources, 196 (2011) 4785-4790.
[34] B. Xu, C.R. Fell, M. Chi, Y.S. Meng, Energy Environ. Sci., 4 (2011) 2223-2233.
[35] Z.D. Li, Y.C. Zhang, H.F. Xiang, X.H. Ma, Q.F. Yuan, Q.S. Wang, C.H. Chen, Journal of Power Sources, 240 (2013) 471-475.
[36] N.-S. Choi, J.-G. Han, S.-Y. Ha, I. Park, C.-K. Back, RSC Advances, 5 (2015) 2732-2748.
[37] Z. Zhang, L. Hu, H. Wu, W. Weng, M. Koh, P.C. Redfern, L.A. Curtiss, K. Amine, Energy Environ. Sci., 6 (2013) 1806-1810.
[38] N. Yabuuchi, K. Yoshii, S.-T. Myung, I. Nakai, S. Komaba, J. Am. Chem. Soc., 133 (2011) 4404-4419.
[39] B. Song, Z. Liu, M.O. Lai, L. Lu, Phys. Chem. Chem. Phys., 14 (2012) 12875-12883.
[40] L. Yang, T. Markmaitree, B.L. Lucht, J. Power Sources, 196 (2011) 2251-2254.
[41] A. von Cresce, K. Xu, J. Electrochem. Soc., 158 (2011) A337-A342.
[42] D.A. Shirley, Physical Review B, 5 (1972) 4709-4714.
[43] J.H. Scofield, Journal of Electron Spectroscopy and Related Phenomena, 8 (1976) 129-137.
[44] S.S. Zhang, K. Xu, T.R. Jow, Journal of Power Sources, 113 (2003) 166-172.
[45] N.D. Nam, I.J. Park, J.-G. Kim, ECS Transactions, 33 (2011) 7-15.
[46] D.H. Doughty, E.P. Roth, C.C. Crafts, G. Nagasubramanian, G. Henriksen, K. Amine, J. Power Sources, 146 (2005) 116-120.
[47] K. Xu, S. Zhang, J.L. Allen, T.R. Jow, J. Electrochem. Soc., 149 (2002) A1079-A1082.
[48] H.-B. Han, S.-S. Zhou, D.-J. Zhang, S.-W. Feng, L.-F. Li, K. Liu, W.-F. Feng, J. Nie, H. Li, X.-J. Huang, M. Armand, Z.-B. Zhou, Journal of Power Sources, 196 (2011) 3623-3632.
[49] S. Menne, R.S. Kühnel, A. Balducci, Electrochimica Acta, 90 (2013) 641-648.
[50] G.C. Allen, S.J. Harris, J.A. Jutson, J.M. Dyke, Applied Surface Science, 37 (1989) 111-134.
[51] J. Hong, H.-D. Lim, M. Lee, S.-W. Kim, H. Kim, S.-T. Oh, G.-C. Chung, K. Kang, Chem. Mater., 24 (2012) 2692-2697.
[52] S.S. Zhang, J. Read, J. Power Sources, 196 (2011) 2867-2870.
[53] D.J. Lee, D. Im, Y.-G. Ryu, S. Lee, J. Yoon, J. Lee, W. Choi, I. Jung, S. Lee, S.-G. Doo, Journal of Power Sources, 243 (2013) 831-835.
[54] L. Dahéron, R. Dedryvère, H. Martinez, M. Ménétrier, C. Denage, C. Delmas, D. Gonbeau, Chemistry of Materials, 20 (2008) 583-590.
[55] H.F. Xiang, H. Wang, C.H. Chen, X.W. Ge, S. Guo, J.H. Sun, W.Q. Hu, J. Power Sources, 191 (2009) 575-581.
[56] Y. Xia, T. Fujieda, K. Tatsumi, P.P. Prosini, T. Sakai, J. Power Sources, 92 (2001) 234-243.
[57] Y. Baba, S. Okada, J.-i. Yamaki, Solid State Ionics, 148 (2002) 311-316.

Tris(2,2,2-trifluoroethyl) phosphite as an electrolyte additive for high-voltage lithium-ion batteries using lithium-rich layered oxide cathode

*Julie Pires[a], Aurore Castets[b], Laure Timperman[a], Jesùs Santos-Peña[a], Erwan Dumont[c], Stéphane Levasseur[d], Cécile Tessier[c], Rémi Dedryvère[b], Mériem Anouti[a]**

(a) Université François Rabelais, Laboratoire PCM2E (EA 6299), Parc de Grandmont

37200 Tours (France)

(b) IPREM (UMR 5254 CNRS), Université de Pau et des Pays de l'Adour, Hélioparc, 2

Avenue Pierre Angot, 64053 Pau Cedex 9 (France)

(c) SAFT, 111 Boulevard Alfred Daney, 33074 Bordeaux Cedex, France

(d) UMICORE, Broekstraat 31, 1000 Brussels, Belgium

Supporting Information

* Corresponding author: E-mail: meriem.anouti@univ-tours.fr, Tel: +33(0)247366951, Fax: +33(0)247367073.

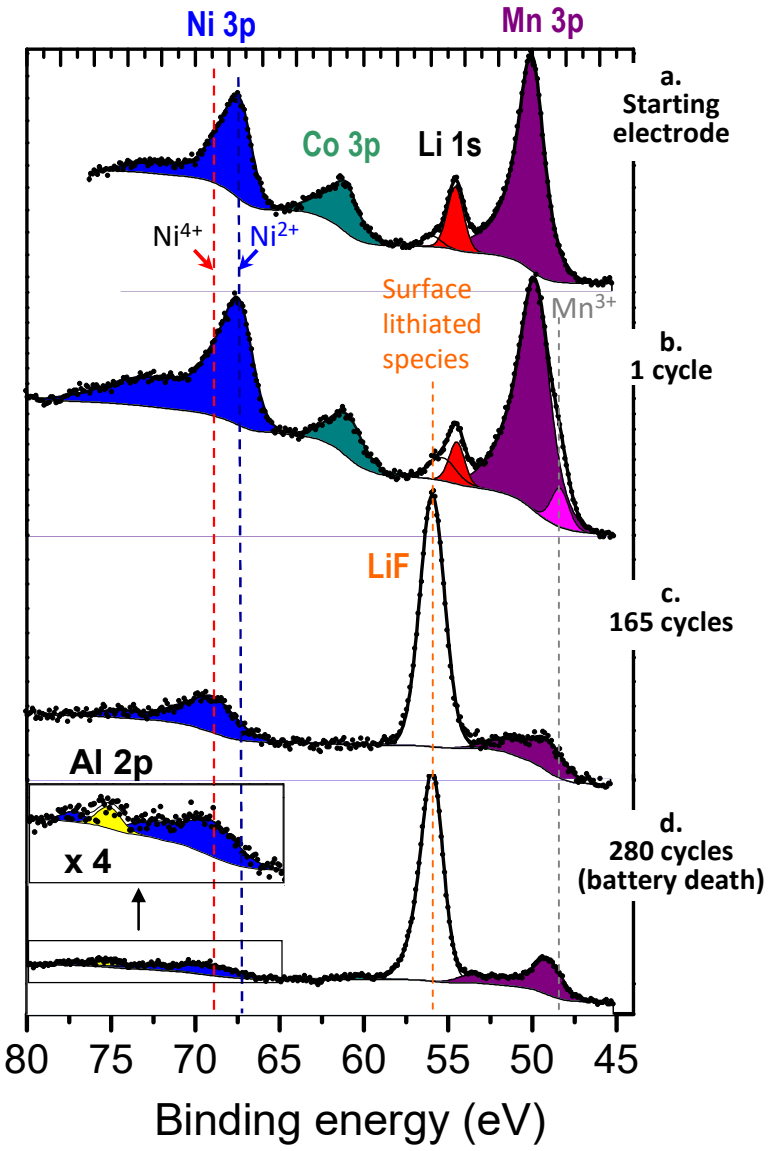

Figure S1: Li 1s, Ni 3p, Co 3p and Mn 3p XPS spectra of positive electrodes cycled in half cells with EC/PC/EMC/DMC + 1M LiPF6 + 5% TTFP electrolyte. Samples as (a) starting electrode (before cycling), and electrodes cycled up to (b) 1 cycle, (c) 165 cycles and (d) 280 cycles (battery death) are compared. Inset corresponds to an enlargement of the spectrum of the 280 cycles sample between 65 and 80 eV.

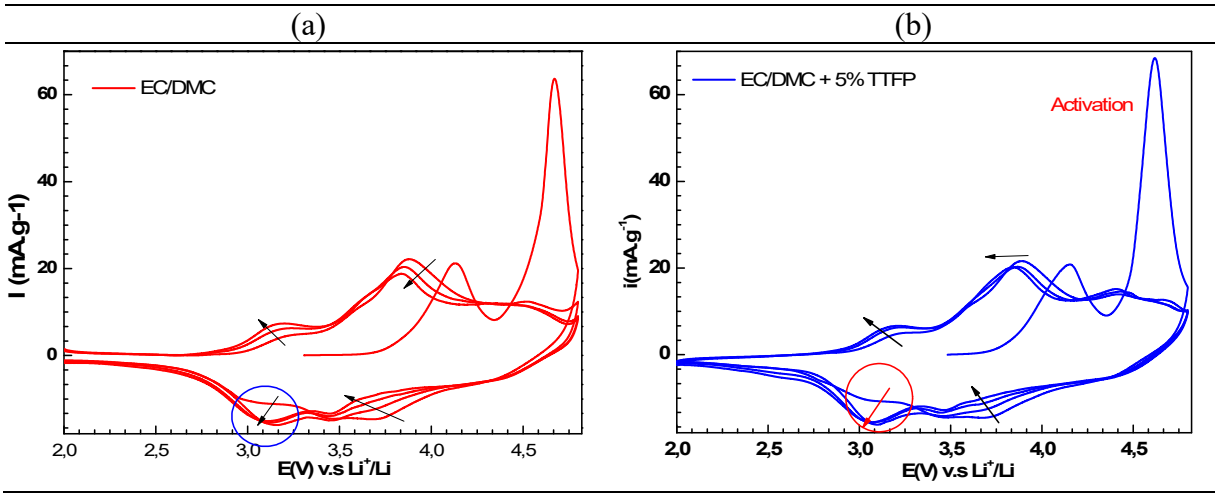

Figure S2 Evolution of CVs during the first four cycles for Li//LR-NMC half-cells with EC/DMC 1M $LiPF_6$ (a), EC/DMC 1M $LiPF_6$ + 5 wt.% TTFP (b), between 2 V and 4,8 V *vs*. Li^+/Li at 20 µV s^{-1}, at room temperature.